Supplementary Information

Ce-Accelerated Spontaneous Redox Synthesis of NiFe-based Electrocatalysts for Efficient Oxygen Evolution Reaction

In-Kyoung Ahn*[1]

[1]Low Carbon Energy Group, Korea Institute of Industrial Technology (KITECH), Ulsan 44413, Republic of Korea

*Correspondence to ikahn@kitech.re.kr (I.-K. Ahn).

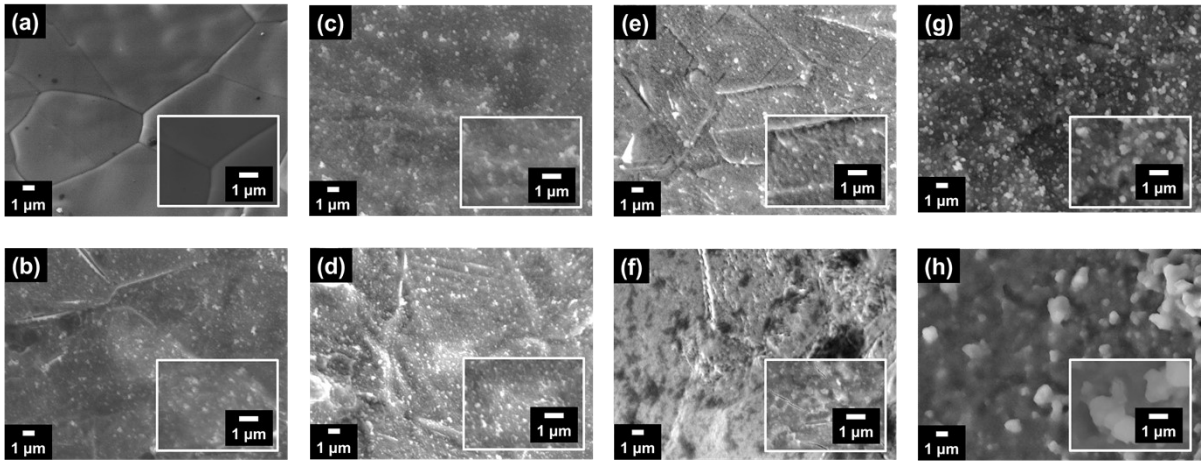

Fig.S1 Low-magnification SEM images with high-magnification insets of (a) nickel foam, (b) Fe-only/NF, (c) FeCe5/NF, (d) FeCe10/NF, (e) FeCe20/NF, (f) FeCe40/NF, (g) Ce-only40/NF, and (h) Ce-only100/NF.

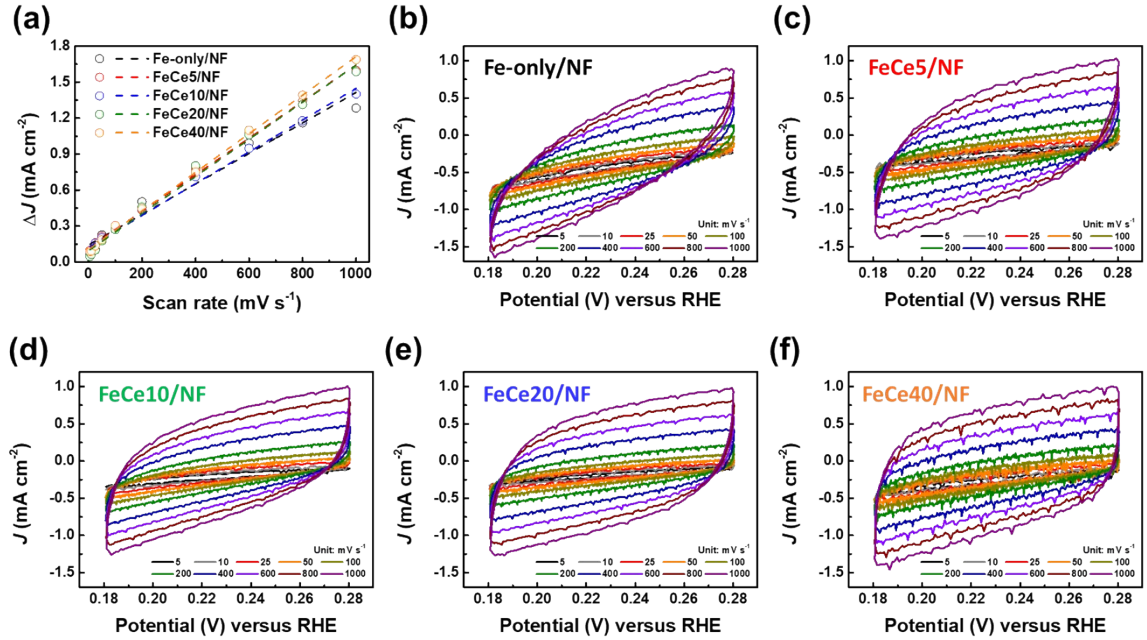

Fig.S2 ECSA analysis of synthesized catalysts to evaluate morphological characteristics. (a) Double-layer capacitance (C_{dl}) measurements derived from linear fits of charging current density vs. scan rate for various NiFe-based electrocatalysts. (b-f) Cyclic voltammetry (CV) curves recorded in the non-Faradaic region for (b) Fe-only/NF, (c) FeCe5/NF, (d) FeCe10/NF, (e) FeCe20/NF, and (f) FeCe40/NF.

The ECSA was estimated by measuring the double-layer capacitance (C_{dl}) in the non-Faradaic region. CV was performed at various scan rates within the potential range of 0.18 to 0.28 V (vs. RHE). The ΔJ (J_a-J_c) at 0.23 V (vs. RHE) was plotted against the scan rate (ν), where the slope of the resulting linear fit corresponds to twice the C_{dl}[S1–S3]. The C_{dl} was calculated using the following equation:

$$C_{dl}=1/2 \times d(\Delta J)/d\nu$$

The ECSA was subsequently determined by normalizing the C_{dl} with the specific capacitance (C_s) of a smooth planar surface[S4–S6]:

$$ECSA=C_{dl}/C_s$$

According to literature, the C_s value for transition metal-based catalysts in 1.0 M KOH electrolyte typically ranges from 20 to 60 μF cm^{-2}. For the purposes of this calculation, a C_s value of 40 μF cm^{-2} was adopted to evaluate and compare the effective surface areas of the electrodes[S4–S6].

Table S1. Comparison of ECSA of prepared electrocatalysts.

Electrocatalysts	Slope	C_{dl}	ECSA
Fe-only/NF	1.27 mF cm^{-2}	0.64 mF cm^{-2}	15.88 cm^2_{ECSA}
FeCe5/NF	1.52 mF cm^{-2}	0.76 mF cm^{-2}	19.00 cm^2_{ECSA}
FeCe10/NF	1.33 mF cm^{-2}	0.67 mF cm^{-2}	16.63 cm^2_{ECSA}
FeCe20/NF	1.55 mF cm^{-2}	0.78 mF cm^{-2}	19.38 cm^2_{ECSA}
FeCe40/NF	1.61 mF cm^{-2}	0.81 mF cm^{-2}	20.13 cm^2_{ECSA}

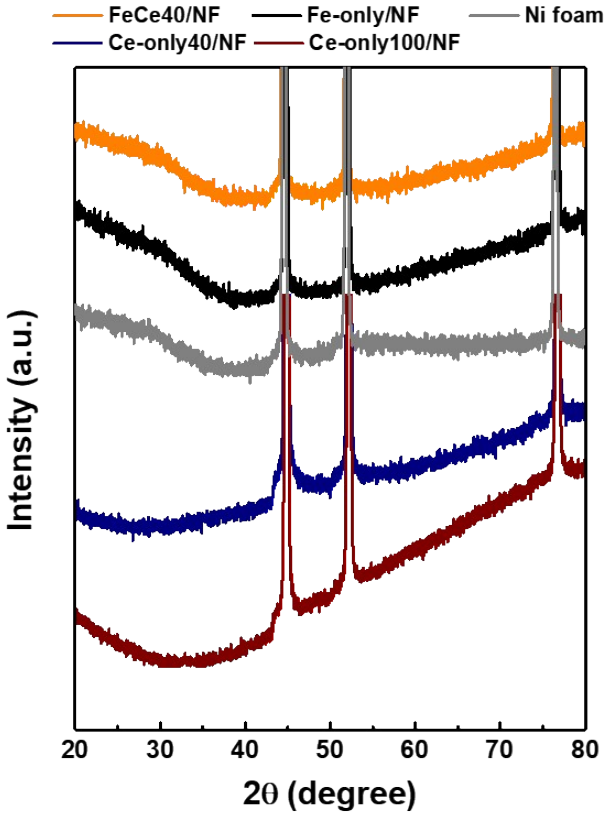

Fig.S3 XRD analysis of the as-prepared electrocatalysts.

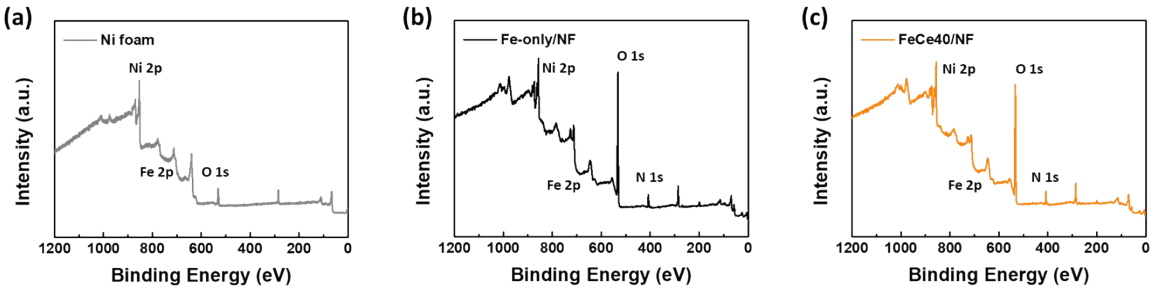

Fig.S4 XPS survey (broad scan) spectra for chemical characterization of (a) Ni foam, (b) Fe-only/NF, and (c) FeCe40/NF.

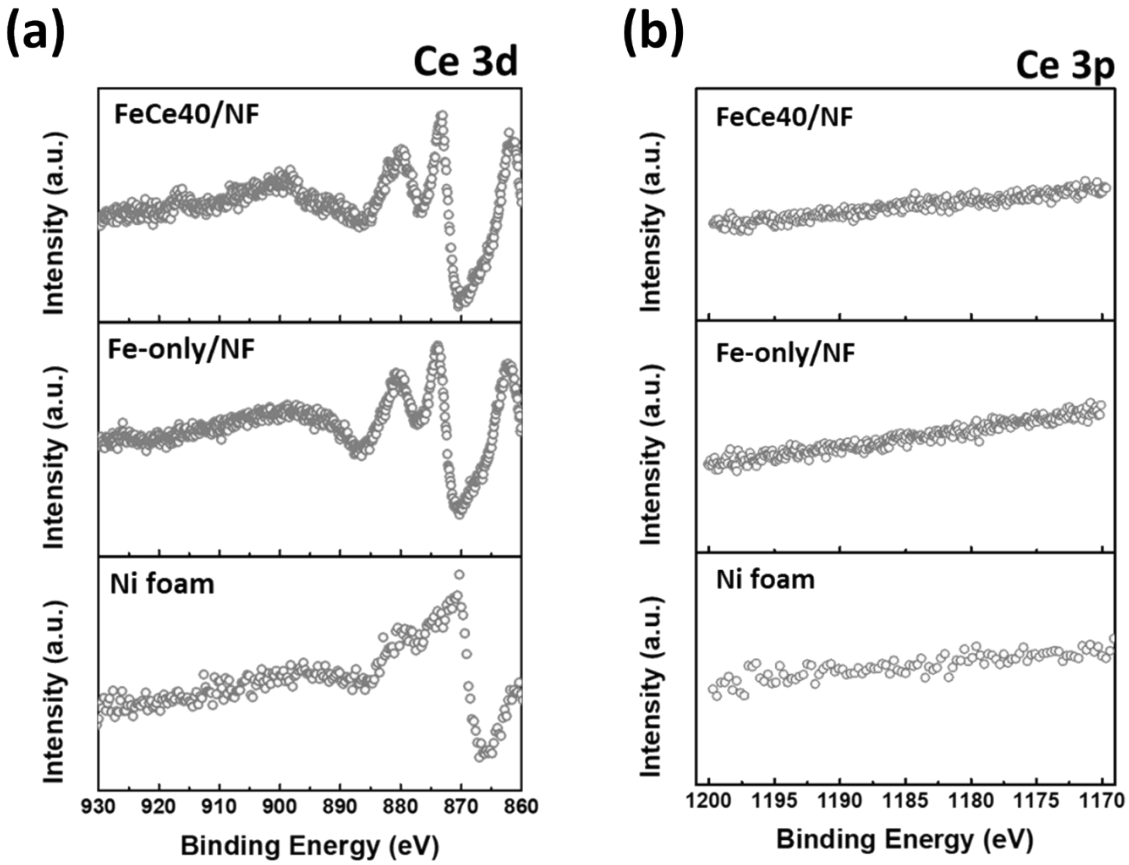

Fig.S5 High-resolution XPS spectra of the (a) Ce 3d and (b) Ce 3p region for the Fe-Ce based electrocatalysts.

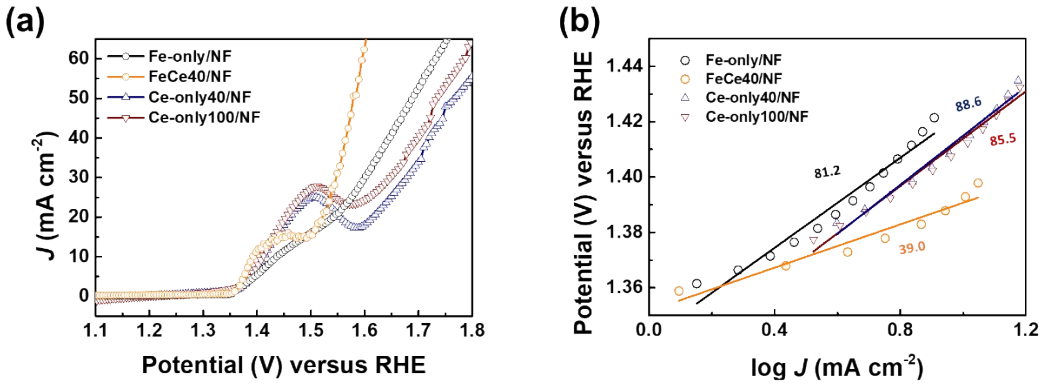

Fig.S6 Comparison of electrochemical OER performance for Fe-only/NF, Ce-only/NF, and FeCe40/NF electrodes. (a) LSV curves recorded in 1.0 M KOH. (b) Corresponding Tafel plots derived from LSV.

Table S2. Equivalent circuit parameters of prepared electrocatalysts.

Electrocatalysts	R_e	R_{ct}	C
Fe-only/NF	5.1 Ω	5.16 Ω	0.032 F
FeCe40/NF	2.1 Ω	4.27 Ω	0.035 F

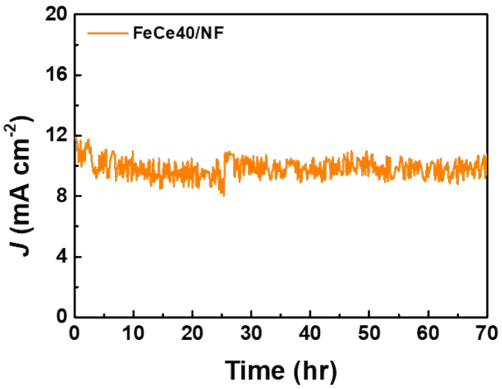

Fig.S7 Long-term stability test of the FeCe40/NF via chronoamperometry at a fixed overpotential of 270 mV (vs. RHE).

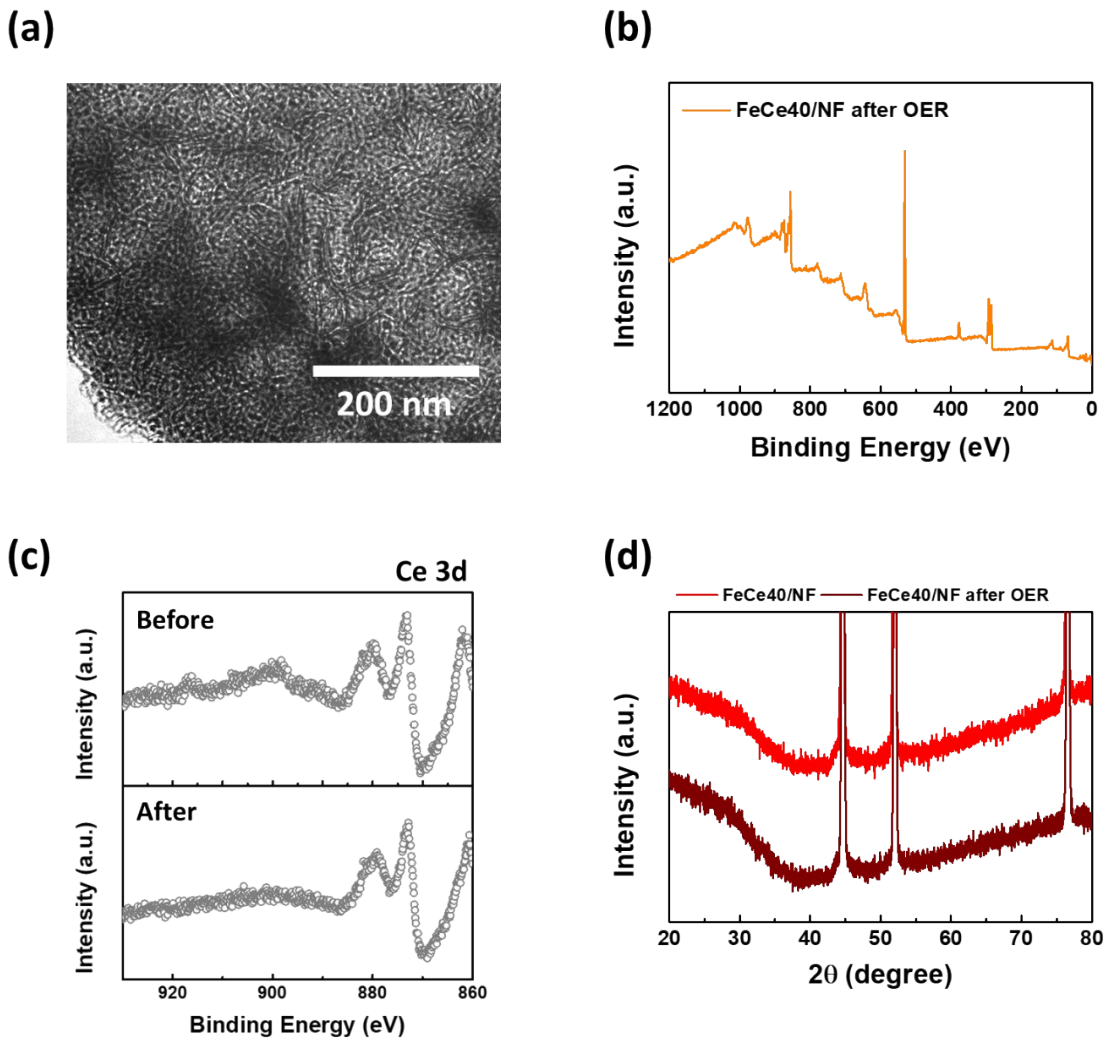

Fig.S8 Post-OER characterization of the electrocatalyst. (a) TEM image after the OER test, (b) XPS survey spectrum after the OER test, (c) comparison of Ce 3d XPS spectra before and after the OER test, and (d) comparison of XRD patterns before and after the OER test.

Table S3. Comparison of OER catalytic activity with previous reports of NiFe-based electrocatalysts.

Catalyst	Synthesis route	Electrolyte	Overpotential (mV)	Current density (mA cm^{-2})	Tafel slopes (mV dec^{-1})	Ref.
FeCe40/NF	Spontaneous redox reaction	1.0 M KOH	349 mV 297 mV	50 mA cm^{-2} 10 mA cm^{-2}	39 mV dec^{-1}	Current work
NiFe-LDH/SnS	Hydrothermal	1.0 M KOH	310	10	53.6	S7
NiFe-LDH/Ti_3C_2	Hydrothermal	1.0 M KOH	334	10	55	S8
NiFe-LDH/$Ni(OH)_2$/NF	Microwave	1.0 M KOH	292	10	84	S9
Ni_3Fe-LDH	Coprecipitation	1.0 M KOH	270	10	43	S10
NiFe-OOH_{OV}	Plasma Exfoliation	1.0 M KOH	270	10	38	S11
Ni_2Fe-Sodium Dodecyl Sulfonate-LDH	Synthetic Intercalation	1.0 M KOH	289	10	38	S12
LDH/oGSH	Composite	0.1 M KOH	350	10	54	S13
Ni_3FeAl_x-LDH	Cationic vacancies	1.0 M KOH	304	20	50	S14
NiFe LDHs-3	Plasma Exfoliation	1.0 M KOH	278	10	87	S15

Dodecyl Sulfate-/NiFe LDH	Anion exchange	1.0 M KOH	300	10	36	S16
NiFe-LDH-15h	Strain tuning	1.0 M KOH	270	10	36	S17
NiFe-Dodecyl Sulfate	Anion exchange	1.0 M KOH	317	10	80	S18
NiFeLa-8 LDH	Electrodeposition	1.0 M KOH	399	50	73	S19
Co^{3+}-NiFe-LDH	Ni and Fe substitution	1.0 M KOH	305	10	59	S20

References

S1 X. Xu, F. Song and X. Hu, A nickel iron diselenide-derived efficient oxygen-evolution catalyst, *Nat. Commun.*, DOI:10.1038/ncomms12324.

S2 H. Deng, C. Zhang, Y. Xie, T. Tumlin, L. Giri, S. P. Karna and J. Lin, Laser induced MoS2/carbon hybrids for hydrogen evolution reaction catalysts, *J. Mater. Chem. A Mater.*, 2016, **4**, 6824–6830.

S3 I. K. Ahn, W. Joo, J. H. Lee, H. G. Kim, S. Y. Lee, Y. Jung, J. Y. Kim, G. B. Lee, M. Kim and Y. C. Joo, Metal-organic Framework-driven Porous Cobalt Disulfide Nanoparticles Fabricated by Gaseous Sulfurization as Bifunctional Electrocatalysts for Overall Water Splitting, *Sci. Rep.*, DOI:10.1038/s41598-019-56084-9.

S4 D. Wang, J. Wang, X. Luo, Z. Wu and L. Ye, In Situ Preparation of Mo2C Nanoparticles Embedded in Ketjenblack Carbon as Highly Efficient Electrocatalysts for Hydrogen Evolution, *ACS Sustain. Chem. Eng.*, 2018, **6**, 983–990.

S5 S. Shit, S. Chhetri, W. Jang, N. C. Murmu, H. Koo, P. Samanta and T. Kuila, Cobalt Sulfide/Nickel Sulfide Heterostructure Directly Grown on Nickel Foam: An Efficient and Durable Electrocatalyst for Overall Water Splitting Application, *ACS Appl. Mater. Interfaces*, 2018, **10**, 27712–27722.

S6 C. C. L. McCrory, S. Jung, I. M. Ferrer, S. M. Chatman, J. C. Peters and T. F. Jaramillo, Benchmarking Hydrogen Evolving Reaction and Oxygen Evolving Reaction Electrocatalysts for Solar Water Splitting Devices, *J. Am. Chem. Soc.*, 2015, **137**, 4347–4357.

S7 Y. Sun, Q. Cai, Z. Wang, Z. Li, Q. Zhou, X. Li, D. Zhao, J. Lu, S. Tian, Y. Li and S. Wang, Two-Dimensional SnS Mediates NiFe-LDH-Layered Electrocatalyst toward Boosting OER Activity for Water Splitting, *ACS Appl. Mater. Interfaces*, 2024, **16**, 23054–23060.

S8 Y. Sun, Z. Wang, Q. Zhou, X. Li, D. Zhao, B. Ding and S. Wang, Ti3C2 mediates the NiFe-LDH layered electrocatalyst to enhance the OER performance for water splitting, *Heliyon*, DOI:10.1016/j.heliyon.2024.e30966.

S9 D. H. Lee, R. Kerkar, D. Arumugam, J. Theerthagiri, S. Ramasamy, S. Kheawhom and M. Y. Choi, Interfacial charge transfer modulation in laser-synthesized catalysts for efficient oxygen evolution, *J. Mater. Chem. A Mater.*, 2024, **12**, 30269–30278.

S10 X. Zhu, M. Du, H. Deng, Y. Liu, J. Chen, S. Wang, H. Li and C. Yan, NiFe layered double hydroxide nanosheets self assembled and etched by phosphotungstic acid for the enhanced oxygen evolution reaction, *Journal of Physics and Chemistry of Solids*, DOI:10.1016/j.jpcs.2024.112143.

S11 Z. Ahmed, Krishankant, R. Rai, R. Kumar, T. Maruyama, C. Bera and V. Bagchi, Unraveling a Graphene Exfoliation Technique Analogy in the Making of Ultrathin

Nickel-Iron Oxyhydroxides@Nickel Foam to Promote the OER, *ACS Appl. Mater. Interfaces*, 2021, **13**, 55281–55291.

S12 H. Zhong, X. Cheng, H. Xu, L. Li, D. Li, P. Tang, N. Alonso-Vante and Y. Feng, Carbon fiber paper supported interlayer space enlarged Ni2Fe-LDHs improved OER electrocatalytic activity, *Electrochim. Acta*, 2017, **258**, 554–560.

S13 X. Zhu, C. Tang, H. F. Wang, Q. Zhang, C. Yang and F. Wei, Dual-sized NiFe layered double hydroxides in situ grown on oxygen-decorated self-dispersal nanocarbon as enhanced water oxidation catalysts, *J. Mater. Chem. A Mater.*, 2015, **3**, 24540–24546.

S14 H. Liu, Y. Wang, X. Lu, Y. Hu, G. Zhu, R. Chen, L. Ma, H. Zhu, Z. Tie, J. Liu and Z. Jin, The effects of Al substitution and partial dissolution on ultrathin NiFeAl trinary layered double hydroxide nanosheets for oxygen evolution reaction in alkaline solution, *Nano Energy*, 2017, **35**, 350–357.

S15 Y. Wang and S. Wang, Ar Plasma Exfoliated Nickel Iron Layered Double Hydroxide Nanosheets into Ultrathin Nanosheets as Highly-Efficient Electrocatalysts for Water Oxidation, *ECS Trans.*, 2017, **80**, 1029–1037.

S16 L. Dang, H. Liang, J. Zhuo, B. K. Lamb, H. Sheng, Y. Yang and S. Jin, Direct Synthesis and Anion Exchange of Noncarbonate-Intercalated NiFe-Layered Double Hydroxides and the Influence on Electrocatalysis, *Chemistry of Materials*, 2018, **30**, 4321–4330.

S17 D. Zhou, S. Wang, Y. Jia, X. Xiong, H. Yang, S. Liu, J. Tang, J. Zhang, D. Liu, L. Zheng, Y. Kuang, X. Sun and B. Liu, NiFe Hydroxide Lattice Tensile Strain: Enhancement of Adsorption of Oxygenated Intermediates for Efficient Water Oxidation Catalysis, *Angewandte Chemie*, 2019, **131**, 746–750.

S18 J. A. Carrasco, R. Sanchis-Gual, A. Seijas-Da Silva, G. Abellan and E. Coronado, Influence of the interlayer space on the water oxidation performance in a family of surfactant-intercalated NiFe-layered double hydroxides, *Chemistry of Materials*, 2019, **31**, 6798–6807.

S19 R. Xu, X. Wang, Z. Yang, Y. Chang, X. Chen, J. Wang and H. Li, Electrodeposition Fabrication of La-Doped NiFe Layered Double Hydroxide to Improve Conductivity for Efficient Overall Water Splitting, *ACS Appl. Energy Mater.*, 2024, **7**, 3866–3875.

S20 Y. Bi, Z. Cai, D. Zhou, Y. Tian, Q. Zhang(m), Q. Zhang(f), Y. Kuang, Y. Li, X. Sun and X. Duan, Understanding the incorporating effect of Co2+/Co3+ in NiFe-layered double hydroxide for electrocatalytic oxygen evolution reaction, *J. Catal.*, 2018, **358**, 100–107.